Analysis of Greenhill Problem by a Co-Rotational Method

Yoshiaki GOTO*, Xiao-Song LI**, Toshihiro KASUGAI*** and Makoto OBATA****

*Professor, Department of Civil Engineering, Nagoya Institute of Technology, Nagoya 466, JAPAN
**Graduate Student, Department of Civil Engineering, Nagoya Institute of Technology, Nagoya 466, JAPAN
***Design Engineer, Design Section, Yokogawa Bridge, Funahashi, Chiba 273, JAPAN
****Associate professor, Department of Civil Engineering, Nagoya Institute of Technology, Nagoya 466, JAPAN

Abstract--The objective of the present study is to theoretically investigate the bifurcation and post-bifurcation behaviors of elastic space rods subject to torsional moment in view of the application to deployable and collapsible members in space structures. This bifurcation phenomena accompanying extremely large rotations in three-dimensional space is referred to as Greenhill problem. We specifically examined how the structural parameters as well as the axial compressive force affect the buckling behaviors. The numerical results obtained here can also be used as severe bench mark checks for geometrically non-linear space frame elements. For this purpose, we developed a versatile FEM-based numerical method using co-rotational technique which has no restrictions on the magnitude of rotations in space. This method yields symmetric tangent stiffness matrix which considerably improves the computational efficiency and accuracy in the bifurcation analysis.

Keywords: Finite rotation, co-rotational method, bifurcation, space frame

1. INTRODUCTION

Bifurcation of elastic rods under torsional moments referred to as Greenhill problem was firstly studied by Greenhill[1], followed by Grammel[2], Ziegler[3] and more recently by Kurakata and Nishino[4], among others. Grammel examined how the magnitude of the buckling moment is influenced by the cross-sectional shapes of the rods. Ziegler investigated the effect of boundary conditions on buckling moment and discussed the kinematic boundary conditions which lead to nonconservative systems.

However, the post-buckling behavior of Greenhill problem has not been studied until quite recently. This is because the post buckling behavior accompanies extremely large rotations in three dimensional space which results in a lot of difficulties in the theoretical approach.

Miura[5] and Natori et al.[6], [7] studied the post-buckling behavior of Greenhill problem in view of the application to the deployable and collapsible members of space structures. Natori et al.[7] examined this post-buckling behavior analytically and experimentally. In his study, Love's governing differential equations [8] for space rods were solved numerically by shooting method. However, the solution procedure adopted by Natori is not based on the incremental equations. This implies that the critical points such as bifurcation points and limits points which exist on the equilibrium path are not precisely identified by their methods. Further, the application of their analysis is restricted to just one numerical example. They did not fully study the effect of structural parameters on the buckling behavior.

The objective of the present study is to precisely examine the buckling behaviors of the Greenhill problem including the post-buckling range. We specifically investigated the effects of cross-sectional shapes as well as the axial compressive force on the buckling behavior. For this purpose, we developed an FEM-based versatile numerical method using co-rotational technique which has no restrictions on the magnitude of rotations in space. This method yields symmetric tangent stiffness matrix which assures the accuracy and efficiency of bifurcation analysis. The numerical results shown here can be also used for the severe bench mark checks of geometrically non-linear space frame elements.

2. ANALYSIS OF RODS ACCOMPANYING LARGE ROTATIONS IN THREE DIMENSIONAL SPACE

In order to investigate the post-buckling behavior of the Greenhill problem, it is necessary to use an accurate method of analysis which precisely takes in account the geometrical nonlinearity, since this post-buckling behavior accompanies extremely large torsional deformations in three dimensional space. The analysis of this kind has been studied by various researchers: Love[8], Antman[9], Bathe and Bolouchi[10], Maeda and Hayashi[11],[12], Yoshida et al.[13], Ai and Nishino[14], Goto, S.[15], Goto, Y. et al.[16], [17], [18], [19], Simo and Vu-Quoc[20], Iura [21],

[22], Iwasaki and Hayashi[23], among others. Although they proposed the theories and numerical methods that might be used to analyze the rods subjected to the extremely large rotations in three-dimensional space, the numerical examples shown by them accompanied only moderate large rotations.

We have developed a numerical method [17] using an incremental transfer matrix technique combined with the arc-length method and applied it to the analysis of deployable and collapsible elastic rings subjected to large rotations in three dimensional space [24]. In this method, the field transfer equations are directly derived from the rigorous governing differential equations of non-linear space rods with Lagrangian expressions[16], [18] and its accuracy is assured. However, the applicability of the transfer matrix method is restricted to simple problems such as the two-boundary value problem. Herein, we developed a versatile FEM-based numerical method based on co-rotational technique. As incremental rotational quantities, we adopted the rotational components around the deformed base vectors which were also used in previous formulations using transfer matrix technique [18]. Adoption of these components which can be treated as vector quantities considerably simplifies the procedure to derive the incremental stiffness equations. Further, the incremental tangent stiffness matrix so derived is symmetric because the theorem of virtual work [25] is used to derive the relation of nodal force components between the co-rotational coordinates and the member coordinates fixed in space.

In what follows, we show the details of our numerical method.

(1) Coordinate systems

The coordinate systems used to derive the member stiffness equation for space rods are shown in Fig. 1. Rectangular Cartesian coordinate system (x,y,z) with base vectors (g_x,g_y,g_z) is introduced at the initial configuration of the member. Orthogonal co-rotational coordinate system

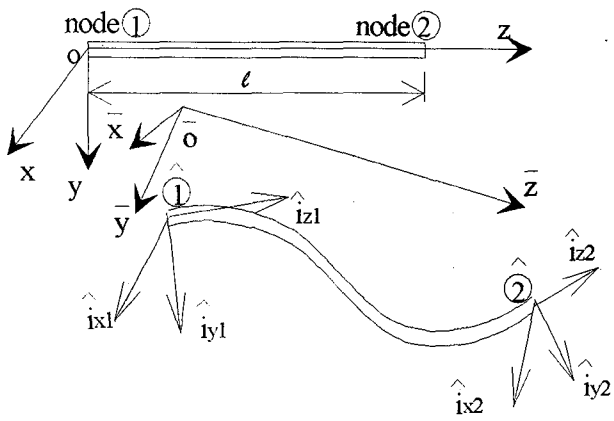

Fig. 1 Coordinate systems

$(\bar{x},\bar{y},\bar{z})$ with base vectors $(\bar{g}_x,\bar{g}_y,\bar{g}_z)$ moves with the rigid body displacements of the space member. The deformed member is expressed by the unit vectors $(\hat{i}_{x_i},\hat{i}_{y_i},\hat{i}_{z_i})$ which are obtained by normalizing the deformed base vectors $(\hat{g}_{x_i},\hat{g}_{y_i},\hat{g}_{z_i})$ at node i.

(2) Components of physical quantities

In this co-rotational formulations, we introduce two sets of nodal force components for a beam element. One is expressed in terms of the member coordinates (x,y,z)as

$$\left\{F_{x_i},F_{y_i},F_{z_i},M_{x_i},M_{y_i},M_{z_i}\right\} \quad (i=1,2) \tag{1}$$

The other is defined with respect to the moving coordinates $(\bar{x},\bar{y},\bar{z})$as

$$\left\{\bar{F}_{x_i},\bar{F}_{y_i},\bar{F}_{z_i},\bar{M}_{x_i},\bar{M}_{y_i},\bar{M}_{z_i}\right\} \quad (i=1,2) \tag{2}$$

Similarly, we use the two sets of nodal displacement components corresponding to the above-defined nodal force components.

$$\left\{U_i,V_i,W_i,\phi_i,\theta_i,\psi_i\right\} \quad (i=1,2) \tag{3}$$

where ϕ_i,θ_i,ψ_i are Eulerian angles in terms of the member coordinates (x,y,z). The components in the moving coordinates $(\bar{x},\bar{y},\bar{z})$ are defined as

$$\left\{\bar{u}_i,\bar{v}_i,\bar{w}_i,\bar{\theta}_{x_i},\bar{\theta}_{y_i},\bar{\theta}_{z_i}\right\} \quad (i=1,2) \tag{4}$$

After the rigid body rotations are removed from the nodal rotations, the remaining rotations become small quantities. Thus, $(\bar{\theta}_{x_i},\bar{\theta}_{y_i},\bar{\theta}_{z_i})$ is considered as the rotations around the moving coordinates axes $(\bar{x},\bar{y},\bar{z})$ and treated as vector quantities.

The components of incremental nodal displacements in the member coordinates (x,y,z) and the moving coordinates $(\bar{x},\bar{y},\bar{z})$ are defined, respectively, as follows

$$\left\{\Delta U_i,\Delta V_i,\Delta W_i,\Delta\theta_{xi},\Delta\theta_{yi},\Delta\theta_{zi}\right\} \quad (i=1,2) \tag{5}$$

$$\left\{\Delta\bar{u}_i,\Delta\bar{v}_i,\Delta\bar{w}_i,\Delta\bar{\theta}_{x_i},\Delta\bar{\theta}_{y_i},\Delta\bar{\theta}_{z_i}\right\} \quad (i=1,2) \tag{6}$$

where $\left(\Delta\theta_{x_i},\Delta\theta_{y_i},\Delta\theta_{z_i}\right)$ are incremental angles around the member coordinate axes. These incremental components are used instead of the increments of Eulerian angles. Although Eulerian angles (ϕ_i,θ_i,ψ_i) are not vector quantities, the incremental angles $\left(\Delta\theta_{x_i},\Delta\theta_{y_i},\Delta\theta_{z_i}\right)$ and $\left(\Delta\bar{\theta}_{x_i},\Delta\bar{\theta}_{y_i},\Delta\bar{\theta}_{z_i}\right)$ can be treated as vector quantities.

(3) Transformation of coordinates

The transformation of the components between the coordinate systems defined in **(1)** can be obtained by using the matrices $[R_i]$ and $[R_G]$ as follows

$$\begin{Bmatrix} \hat{i}_{x_i} \\ \hat{i}_{y_i} \\ \hat{i}_{z_i} \end{Bmatrix} = [R_i] \begin{Bmatrix} g_x \\ g_y \\ g_z \end{Bmatrix} \quad (i=1,2), \quad \begin{Bmatrix} \bar{i}_x \\ \bar{i}_y \\ \bar{i}_z \end{Bmatrix} = [R_G] \begin{Bmatrix} g_x \\ g_y \\ g_z \end{Bmatrix} \tag{7,8}$$

$[R_i]$, and $[R_G]$ are expressed by Eulerian angles $(\phi_i,\ \theta_i,\ \psi_i)$ and $(\bar{\phi}\ ,\ \bar{\theta}\ ,\ \bar{\psi}\ )$ as

$$[R_i] = [TR(\phi_i, \theta_i, \psi_i)] \quad (i=1,2) \tag{9}$$

$$[R_G] = [TR(\bar{\phi}\ ,\bar{\theta}\ ,\bar{\psi}\ )] \tag{10}$$

where

$$\bar{\phi} = (\phi_1+\phi_2)/2, \bar{\theta} = (\theta_1+\theta_2)/2, \bar{\psi} = (\psi_1+\psi_2)/2 \tag{11}$$

and

$$[TR(a,b,c)] = \begin{bmatrix} 1 & 0 & 0 \\ 0 & \cos a & \sin a \\ 0 & -\sin a & \cos a \end{bmatrix} \times \begin{bmatrix} \cos b & 0 & -\sin b \\ 0 & 1 & 0 \\ -\sin b & 0 & \cos b \end{bmatrix} \times \begin{bmatrix} \cos c & \sin c & 0 \\ -\sin c & \cos c & 0 \\ 0 & 0 & 1 \end{bmatrix} \tag{12}$$

Eqn(11) implies that the directions of the moving coordinates $(\bar{i}_x, \bar{i}_y, \bar{i}_z)$ is defined by the averaged Eulerian angles of $(\hat{i}_{x_1}, \hat{i}_{y_1}, \hat{i}_{z_1})$ and $(\hat{i}_{x_2}, \hat{i}_{y_2}, \hat{i}_{z_2})$. From eqns (7) and (8), the following relation can be obtained.

$$\begin{Bmatrix} \hat{i}_{x_i} \\ \hat{i}_{y_i} \\ \hat{i}_{z_i} \end{Bmatrix} = [R_i][R_G]^t \begin{Bmatrix} \bar{i}_x \\ \bar{i}_y \\ \bar{i}_z \end{Bmatrix} \quad (i=1,2) \tag{13}$$

(4) Transformation of rotational components

Since $(\bar{\theta}_{x_i}, \bar{\theta}_{y_i}, \bar{\theta}_{z_i})$ is regarded as vector quantities, the relation between $(\hat{i}_{x_i}, \hat{i}_{y_i}, \hat{i}_{z_i})$ and $(\bar{i}_x, \bar{i}_y, \bar{i}_z)$ can also be expressed as

$$\begin{Bmatrix} \hat{i}_{x_i} \\ \hat{i}_{y_i} \\ \hat{i}_{z_i} \end{Bmatrix} = \begin{bmatrix} 1 & \bar{\theta}_{z_i} & -\bar{\theta}_{y_i} \\ -\bar{\theta}_{z_i} & 1 & \bar{\theta}_{x_i} \\ \bar{\theta}_{y_i} & -\bar{\theta}_{x_i} & 1 \end{bmatrix} \begin{Bmatrix} \bar{i}_x \\ \bar{i}_y \\ \bar{i}_z \end{Bmatrix} \quad (i=1,2) \tag{14}$$

From eqns (7), (8) and (14), we have the following relation

$$[R_i][R_G]^t = \begin{bmatrix} 1 & \bar{\theta}_{z_i} & -\bar{\theta}_{y_i} \\ -\bar{\theta}_{z_i} & 1 & \bar{\theta}_{x_i} \\ \bar{\theta}_{y_i} & -\bar{\theta}_{x_i} & 1 \end{bmatrix} \quad (i=1,2) \tag{15}$$

Considering that the relative rotations between node 1 and node 2 are small, we have the following relations

$$|\phi_1 - \phi_2| << 1\ ,\ |\theta_1 - \theta_2| << 1\ ,\ |\psi_1 - \psi_2| << 1 \tag{16}$$

Substituting eqn(16) into $[R_i][R_G]^t$ and comparing the both sides of eqn (15), the relation between $(\bar{\theta}_{x_i}, \bar{\theta}_{y_i}, \bar{\theta}_{z_i})$ and $(\phi_i, \theta_i, \psi_i)$ can be obtained as

$$\begin{Bmatrix} \bar{\theta}_{x_1} \\ \bar{\theta}_{y_1} \\ \bar{\theta}_{z_1} \end{Bmatrix} = -\begin{Bmatrix} \bar{\theta}_{x_2} \\ \bar{\theta}_{y_2} \\ \bar{\theta}_{z_2} \end{Bmatrix} = \frac{1}{2}[BR(\bar{\theta}, \bar{\phi})] \left(\begin{Bmatrix} \phi_1 \\ \theta_1 \\ \psi_1 \end{Bmatrix} - \begin{Bmatrix} \phi_2 \\ \theta_2 \\ \psi_2 \end{Bmatrix} \right) \tag{17}$$

where

$$[BR(\bar{\theta}, \bar{\phi})] = \begin{bmatrix} 1 & 0 & -\sin\bar{\theta} \\ 0 & \cos\bar{\phi} & \cos\bar{\theta}\sin\bar{\phi} \\ 0 & -\sin\bar{\phi} & \cos\bar{\theta}\cos\bar{\phi} \end{bmatrix} \tag{18}$$

The relation between $(\Delta\theta_{x_i}, \Delta\theta_{y_i}, \Delta\theta_{z_i})$ and $(\Delta\bar{\theta}_{x_i}, \Delta\bar{\theta}_{y_i}, \Delta\bar{\theta}_{z_i})$ is derived in the following. Because $(\Delta\hat{\theta}_{x_i}, \Delta\hat{\theta}_{y_i}, \Delta\hat{\theta}_{z_i})$ are the small incremental rotations around $(\hat{i}_{x_i}, \hat{i}_{y_i}, \hat{i}_{z_i})$ $(i=1,2)$, we have

$$\{\hat{i}_{x_i}, \hat{i}_{y_i}, \hat{i}_{z_i}\} \begin{Bmatrix} \Delta\hat{\theta}_{x_i} \\ \Delta\hat{\theta}_{y_i} \\ \Delta\hat{\theta}_{z_i} \end{Bmatrix} = \{g_{x_i}, g_{y_i}, g_{z_i}\} \begin{Bmatrix} \Delta\theta_{x_i} \\ \Delta\theta_{y_i} \\ \Delta\theta_{z_i} \end{Bmatrix} \quad (i=1,2) \tag{19}$$

Thus, eqns (7) and (19) lead to

$$\begin{Bmatrix} \Delta\hat{\theta}_{x_i} \\ \Delta\hat{\theta}_{y_i} \\ \Delta\hat{\theta}_{z_i} \end{Bmatrix} = [R_i] \begin{Bmatrix} \Delta\theta_{x_i} \\ \Delta\theta_{y_i} \\ \Delta\theta_{z_i} \end{Bmatrix} \quad (i=1,2) \tag{20}$$

On the other hand, the increments of the vectors $(\hat{i}_{x_i}, \hat{i}_{y_i}, \hat{i}_{z_i})$ are expressed by using $(\Delta\hat{\theta}_{x_i}, \Delta\hat{\theta}_{y_i}, \Delta\hat{\theta}_{z_i})$ as follows

$$\begin{Bmatrix} \Delta\hat{i}_{x_i} \\ \Delta\hat{i}_{y_i} \\ \Delta\hat{i}_{z_i} \end{Bmatrix} = \begin{bmatrix} 0 & \Delta\hat{\theta}_{z_i} & -\Delta\hat{\theta}_{y_i} \\ -\Delta\hat{\theta}_{z_i} & 0 & \Delta\hat{\theta}_{x_i} \\ \Delta\hat{\theta}_{y_i} & -\Delta\hat{\theta}_{x_i} & 0 \end{bmatrix} \begin{Bmatrix} \hat{i}_{x_i} \\ \hat{i}_{y_i} \\ \hat{i}_{z_i} \end{Bmatrix} \quad (i=1,2) \tag{21}$$

Taking the increment of eqn(7) and comparing with eqn (21), we have

$$\begin{Bmatrix} \Delta\hat{\theta}_{x_i} \\ \Delta\hat{\theta}_{y_i} \\ \Delta\hat{\theta}_{z_i} \end{Bmatrix} = \left[BR(\theta_i,\phi_i)\right] \begin{Bmatrix} \Delta\phi_i \\ \Delta\theta_i \\ \Delta\psi_i \end{Bmatrix} \qquad (i=1,2) \tag{22}$$

Finally, eqns (20) and (22) yield

$$\begin{Bmatrix} \Delta\theta_{x_i} \\ \Delta\theta_{y_i} \\ \Delta\theta_{z_i} \end{Bmatrix} = \left[R_i\right]^t \left[BR(\theta_i,\phi_i)\right] \begin{Bmatrix} \Delta\phi_i \\ \Delta\theta_i \\ \Delta\psi_i \end{Bmatrix} \quad (i=1,2) \tag{23}$$

Therefore, from eqns (17) and (23), we obtain

$$\begin{Bmatrix} \Delta\bar{\theta}_{x_1} \\ \Delta\bar{\theta}_{y_1} \\ \Delta\bar{\theta}_{z_1} \end{Bmatrix} = -\begin{Bmatrix} \Delta\bar{\theta}_{x_2} \\ \Delta\bar{\theta}_{y_2} \\ \Delta\bar{\theta}_{z_2} \end{Bmatrix} = \left[DR_1\right]\left[BR(\theta_1,\phi_1)\right]^{-1}\left[R_1\right] \begin{Bmatrix} \Delta\theta_{x_1} \\ \Delta\theta_{y_1} \\ \Delta\theta_{z_1} \end{Bmatrix} + \left[DR_2\right]\left[BR(\theta_2,\phi_2)\right]^{-1}\left[R_2\right] \begin{Bmatrix} \Delta\theta_{x_2} \\ \Delta\theta_{y_2} \\ \Delta\theta_{z_2} \end{Bmatrix} \tag{24}$$

($\left[DR_1\right], \left[DR_2\right]$ see Appendix (a)).

(5) Transformation of translational displacements

If the origin of the moving coordinates is chosen to coincide with the node 1 of the deformed member, the following equation holds

$$\left(\bar{u}_1, \bar{v}_1, \bar{w}_1\right) = 0 \tag{25}$$

Thus,

$$\begin{Bmatrix} \bar{u}_2 \\ \bar{v}_2 \\ \bar{w}_2 + l \end{Bmatrix} = \left[R_G\right] \begin{Bmatrix} u_2 - u_1 \\ v_2 - v_1 \\ w_2 - w_1 + l \end{Bmatrix} \tag{26}$$

where l is the original length of the member. Taking the increment of eqn(26) and using eqn(23), the following relation can be obtained.

$$\begin{Bmatrix} \Delta\bar{u}_2 \\ \Delta\bar{v}_2 \\ \Delta\bar{w}_2 \end{Bmatrix} = \left[Et_1\right] \begin{Bmatrix} \Delta\theta_{x_1} \\ \Delta\theta_{y_1} \\ \Delta\theta_{z_1} \end{Bmatrix} + \left[Et_2\right] \begin{Bmatrix} \Delta\theta_{x_2} \\ \Delta\theta_{y_2} \\ \Delta\theta_{z_2} \end{Bmatrix} + \left[R_G\right] \left(\begin{Bmatrix} \Delta u_2 \\ \Delta v_2 \\ \Delta w_2 \end{Bmatrix} - \begin{Bmatrix} \Delta u_1 \\ \Delta v_1 \\ \Delta w_1 \end{Bmatrix} \right) \tag{27}$$

($\left[Et_1\right], \left[Et_2\right]$ see Appendix (b))

From eqns (24) and (27), we have the relation of incremental displacements and rotations between the member coordinates (x,y,z) and moving coordinates $(\bar{x},\bar{y},\bar{z})$ as

$$\begin{Bmatrix} \Delta\bar{u}_2 \\ \Delta\bar{v}_2 \\ \Delta\bar{w}_2 \\ \Delta\bar{\theta}_{x_2} \\ \Delta\bar{\theta}_{y_2} \\ \Delta\bar{\theta}_{z_2} \end{Bmatrix} = \left[R\right] \begin{Bmatrix} \Delta u_1, \Delta v_1, \Delta w_1, \Delta\theta_{x_1}, \Delta\theta_{y_1}, \Delta\theta_{z_1}, \\ \Delta u_2, \Delta v_2, \Delta w_2, \Delta\theta_{x_2}, \Delta\theta_{y_2}, \Delta\theta_{z_2} \end{Bmatrix}^t \tag{28}$$

where $\left[R\right]$ is shown in Appendix (c)

(6) Derivation of incremental tangent stiffness equations

The stiffness equation in the moving coordinates are simplified with the help of eqn (25) as follows

$$\begin{Bmatrix} \bar{F}_{x_2} \\ \bar{F}_{y_2} \\ \bar{F}_{z_2} \\ \bar{M}_{x_2} - \bar{M}_{x_1} \\ \bar{M}_{y_2} - \bar{M}_{y_1} \\ \bar{M}_{z_2} - \bar{M}_{z_1} \end{Bmatrix} = E/l^3 \begin{bmatrix} 12I_{yy} & & & & & \\ & 12I_{xx} & & & 0 & \\ & & Al^2 & & & \\ & & & 4I_{xx}l^2 & & \\ & & & & 4I_{yy}l^2 & \\ & 0 & & & & 4Gkl^2/E \end{bmatrix} \begin{Bmatrix} \bar{u}_2 \\ \bar{v}_2 \\ \bar{w}_2 \\ \bar{\theta}_{x_2} \\ \bar{\theta}_{y_2} \\ \bar{\theta}_{z_2} \end{Bmatrix}$$

or

$$\left\{\bar{f}\right\} = \left[\bar{k}\right]\left\{\bar{u}\right\} \tag{29}$$

The above equation is based on the small displacement theory because the displacement components $\left(\bar{u}_i, \bar{v}_i, \bar{w}_i, \bar{\theta}_{x_i}, \bar{\theta}_{y_i}, \bar{\theta}_{z_i}\right)$ defined in the moving coordinates is considered small.

The equation of virtual work [25] leads to

$$\delta\{u\}^t\{f\} = \delta\{\bar{u}\}^t\{\bar{f}\} \tag{30}$$

where

$$\delta\{u\}^t = \left\{\delta u_1, \delta v_1, \delta w_1, \delta\theta_{x_1}, \delta\theta_{y_1}, \delta\theta_{z_1}, \delta u_2, \delta v_2, \delta w_2, \delta\theta_{x_2}, \delta\theta_{y_2}, \delta\theta_{z_2}\right\}$$
$$\{f\} = \left\{F_{x_1}, F_{y_1}, F_{z_1}, M_{x_1}, M_{y_1}, M_{z_1}, F_{x_2}, F_{y_2}, F_{z_2}, M_{x_2}, M_{y_2}, M_{z_2}\right\}$$

Substituting eqns (28) and (29) into eqn (30), we have the following relation

$$\{f\} = \left[R\right]\left\{\bar{f}\right\} \tag{31}$$

The tangent stiffness equation can be derived by taking the increment of eqn (31) as

$$\Delta\{f\} = \left[\Delta k\right]\Delta\{u\} \tag{32}$$

where $[\Delta k]$ is a symmetric tangent stiffness matrix.

Eqn (32) is the generalized incremental stiffness equation in the member coordinates. The transformation from the member coordinates to the global coordinates fixed in space is the same as that of the usual finite element method. The nonlinear algebraic equations are solved by the arc-length method combined with the Newton-Raphson iterative procedures.

3. ACCURACY OF THE PROPOSED METHOD

The elastic buckling behaviors of deployable and collapsible rings studied by Goto et al.[24] accompany very large rotations in three dimensional space. Herein, we use this example to examine the accuracy of the present co-rotational method.

The ring model and global coordinates are shown in Fig.2. By virtue of the symmetry of the structure, only the half of the original model is analyzed. In the example, we chose a ring with a rectangular cross-section whose structural parameters are $h/b=3$, and $R/h=20$. It is important to know how many elements are necessary to obtain the convergent solutions. In this numerical example, 20, 80, 120, and 200 elements are used.

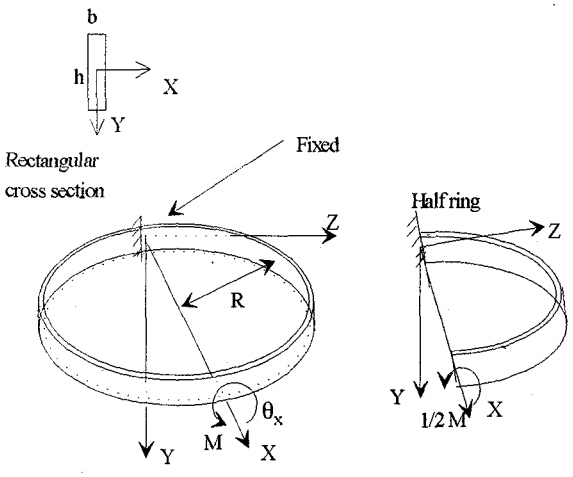

Fig.2 Ring model and global coordinates

The numerical results are given in Fig.3 in comparison with the analytical solution [24]. The deformed shapes of the ring are also illustrated in Fig.4. From Fig.3, we can observe that the numerical solution almost converges to the analytical solution when the number of finite elements increases up to 200. This implies that the proposed co-rotational method has a good accuracy compared with the analytical solution.

4. ANALYSIS OF GREENHILL PROBLEM

(1) Bifurcation analysis

The stability of a structural system is lost due to the existence of singular points on the equilibrium path, referred to as critical points, i.e., bifurcation points and limit points. At bifurcation points, the solution of a structural tangent stiffness ceases to be unique for a given load condition and becomes singular. For a perfect structural system, it is assumed that the incremental overall stiffness equations on a fundamental path and on a bifurcation path are respectively

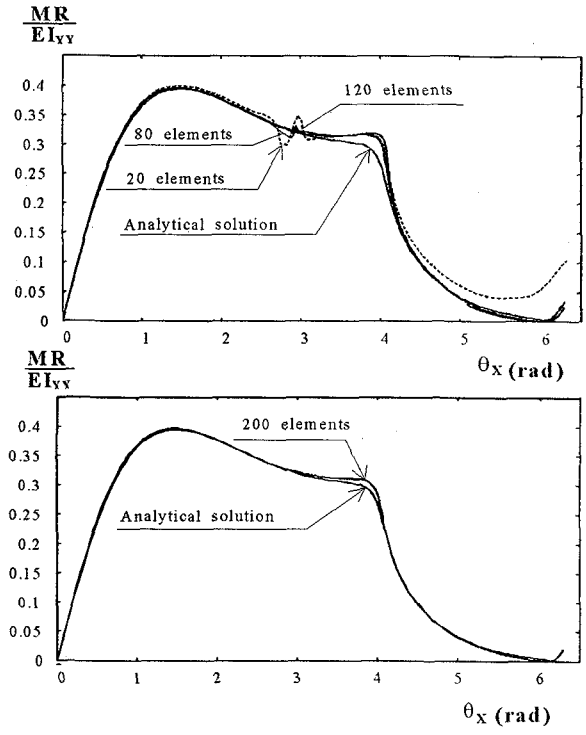

Fig.3 Moment-rotation curves of the ring with h/b=3 and R/h=20

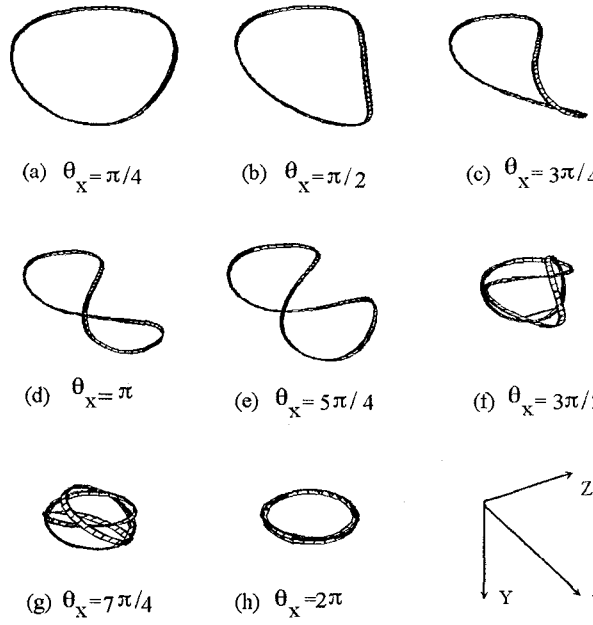

Fig.4 Deformed shapes of the deployable ring

expressed by summation convention as follows at a bifurcation point:

$$\Delta\{f\}=[\Delta k]\Delta\{u^f\},\quad \Delta\{f\}=[\Delta k]\Delta\{u^b\} \tag{33-a,b}$$

where superscripts f and b denote the quantities on the fundamental path and the bifurcation path, respectively.

At the bifurcation point, both eqns (33-a) and (33-b) hold simultaneously, thus resulting in the following equation

$$:[\Delta k]\left(\Delta\{u^b\}-\Delta\{u^f\}\right)=0 \tag{34}$$

Since $\left(\Delta\{u^b\}-\Delta\{u^f\}\right)$ is not zero, eqn (34) holds only when $|\Delta k|=0$ and $\left(\Delta\{u^b\}-\Delta\{u^f\}\right)$ coincides with the eigenvector of $[\Delta k]$.

For elastic space rods with a symmetric bifurcation (pitchfork bifurcation point) where the bifurcation occurs without the change of applied loads, eqn(33-b) is reduced to

$$\Delta\{f\}=[\Delta k]\Delta\{u^b\}=0 \tag{35}$$

Thus, the incremental displacement $\Delta\{u^b\}$ along the bifurcation path can be obtained as the eigenvector of $[\Delta k]$.

In what follows, we use both analytical method [26] and the present numerical method to study the buckling behavior of elastic space rods under torsional moment.

(2) Numerical example

Herein, we precisely examine the buckling behavior of Greenhill problem. The structural model used for the present analysis is shown in Fig.5. The boundary conditions of the rod are the same as those of the model analyzed by Natori [7]. Since the torsional moment applied to this model is conservative, a static analysis yields a correct buckling load. We examine the rods with rectangular cross-section as well as the round cross-section. The constants for the rectangular cross-section are given by

$$A=bh,\quad I_{xx}=b^3h/12,\quad I_{yy}=bh^3/12,$$
$$J=\frac{b^3h}{3}\left\{1-\frac{192b}{\pi^5h}\sum_{n=1}^{\infty}\frac{1}{(2n-1)^5}\tanh\frac{(2n-1)\pi h}{2b}\right\} \tag{36a-e}$$
$$E/G=2.6$$

(Timoshenko et al.[27])

If we use the non-dimensionalized torsional moment $M_z l/E(I_{xx}+I_{yy})/2$ as a load parameter, the governing structural parameter for rectangular cross-section is reduced to h/b.

3) Buckling behavior of elastic space rods with different cross-sections

Buckling behavior of elastic rods with circular cross-section under torsional load was firstly studied by Greenhill. According to him, the buckling moment is expressed by

$$M_{cr}=\pm k\frac{\pi}{l}EI,\quad I=\frac{\pi r^4}{4} \tag{37-a,b}$$

where k is a constant which is dependent on boundary conditions. In case of the rod illustrated in Fig.5, k = 2.861

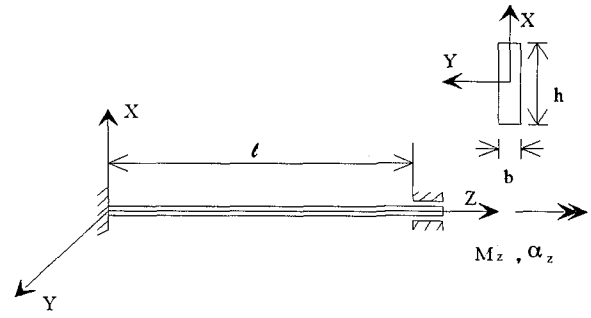

Fig.5 Analysis model

and the corresponding non-dimensional buckling moment $M_z l/E(I_{xx}+I_{yy})/2$ is equal to 8.988. For the rod with rectangular cross-section, the buckling phenomenon is caused by a distinct bifurcation point existing on the equilibrium path. Thus, the buckling moment can be calculated numerically by the condition that the determinant of the tangent stiffness matrix $|\Delta k|$ changes its sign from plus to minus at the branching point. However, $|\Delta k|$ for rods with circular cross-section does not change its sign, although $|\Delta k|$ becomes zero at this branching point. This is because the two eigenvalues of the tangent stiffness matrix become zero simultaneously when the bifurcation occurs. This bifurcation point, referred to as coincident bifurcation point, has to be identified by examining the change of the sign of the eigenvalues. With the aforementioned method, the buckling moments of space torsional rods with different h/b are obtained by both analytical method [26] and the present co-rotational method as shown in Fig.6.

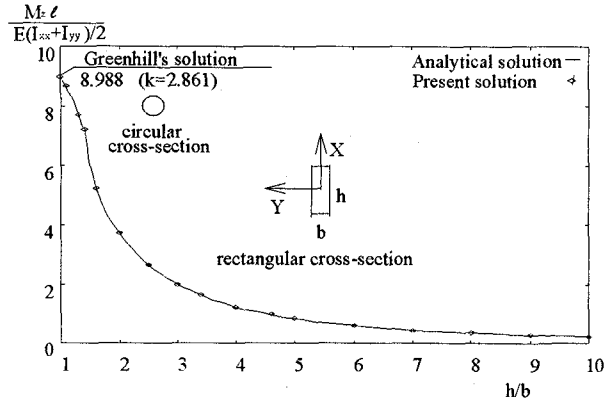

Fig.6 Buckling moments of space rods with different cross-section

From Fig.6, it can be seen that buckling moments are much influenced by the parameter h/b, that is, the buckling moments decrease with the increase of the structural parameter h/b. It can be also seen that the present numerical method yields accurate bifurcation moment compared with those of the analytical solution.

(4) Effect of compressive force on buckling moment

As is well known, the axial compressive force decreases the buckling moment. Herein, we choose the non-dimensional axial compressive force with the values of $Pl^2/\pi^2 EI_{xx}$=0.3 and 0.5, as the initial load parameters, to investigate their effect on buckling moment. The results are shown in Fig.7. It is observed from Fig.7 that the axial compressive force has little effect on buckling loads when $h/b \geq 4$. Only the shapes of cross-section govern the values of buckling loads when $h/b \geq 4$.

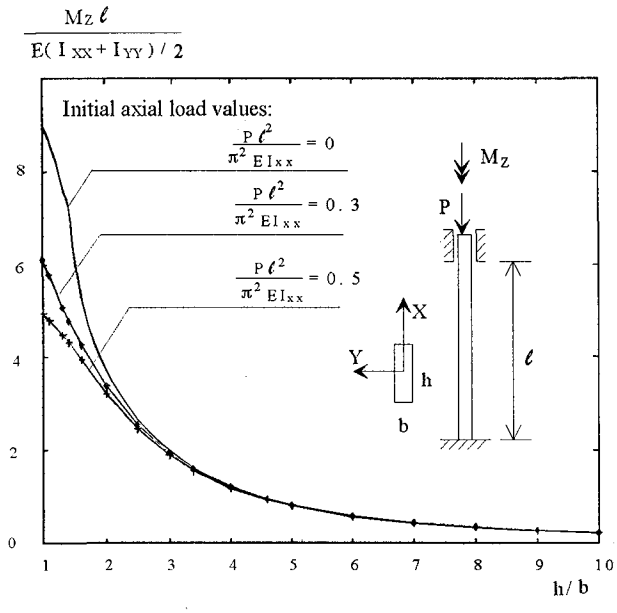

Fig.7 Effect of axial compressive force on buckling moments

(5) Tracing of bifurcation path

With the co-rotational method explained in section 2, we analyzed and traced the post-bifurcation paths of rods subject to torsional moment.

For a perfect system, the incremental displacements along the bifurcation path are obtained as the eigenvector of tangent stiffness matrix $[\Delta k]$. Fig.8 shows the bifurcation paths of rods with 5 types of cross-sections, where w_0 is the axial displacement of the loaded-end and l is the original length of the rod.

Specifically, for the case of $h/b=3$, we trace the bifurcation paths not only at the first bifurcation point, but also at the secondary bifurcation point as illustrated in Fig.9. The deformation of the rod are shown in Fig.10. In Fig.9, point (c) is the first bifurcation point and curve (c)-(d)-(e)-(f) is the first bifurcation path. At point (f), the secondary bifurcation occurs. From point (f), two paths are traced. One is a path (f)-(p)-(q)-(r)-(t)-(u), the other is a path (f)-(g)-(h)-(i)-(j). In order to ascertain which one is the first bifurcation path, the deformed shapes at 3 points on the equilibrium path are compared, that is, points (x1), (x2), (x3) which are adjacent to the first bifurcation point (f) as shown in Fig.9. As is well known, the deformed shape of space rods is symmetric at the first bifurcation point, and this symmetry will be kept along the first bifurcation path. However, the symmetry will be lost if the deformation follows the secondary bifurcation path. Since it is difficult to find out a symmetric axis especially for deformed rods, projections of

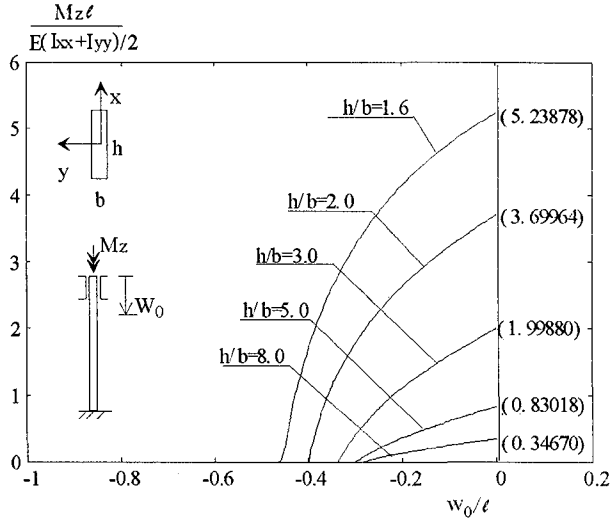

Fig.8 Post-bifurcation behavior of rectangular bar

deformed shapes onto X-Y and Y-Z planes are compared at the 3 points on the equilibrium paths as illustrated in Fig.11. The symmetry is kept at point (x3), while that is lost at point (x2). Therefore, the curve (f)-(p)-(q)-(r)-(t)-(u) is identified as the first bifurcation path, while the curve (f)-(g)-(h)-(i)-(j) is the secondary bifurcation path.

5. CONCLUDING REMARKS

In the present paper, we have presented a co-rotational method for space frame analysis which precisely took into account the geometric non-linearity without restrictions on the magnitude of finite rotations in three-dimensional space. As an numerical example to examine its accuracy, the buckling behavior of a deployable and collapsible ring was calculated. The results showed that the method had a good accuracy compared with the analytical solution if an appropriate number of finite elements were used.

With the co-rotational method so developed, we analyzed the Greenhill problem. It is observed from the numerical analysis that in the case of $h/b<4$, the buckling moments decrease when h/b or/and axial compressive force is increased. In the case of $h/b \geq 4$, the axial compressive force has little effect on buckling moments and only the structural parameter h/b governs the values of buckling moments.

Regarding the post-bifurcation behaviors of a perfect system, it is confirmed that bifurcation occurs again on the first bifurcation path.

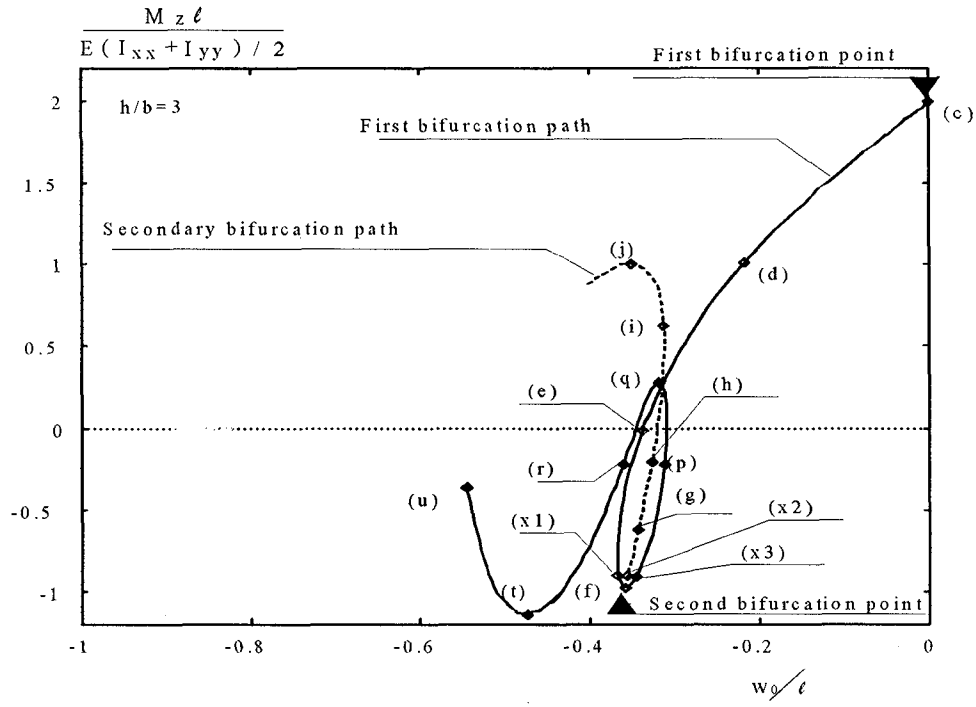

Fig.9 Tracing of bifurcation path with h/b=3

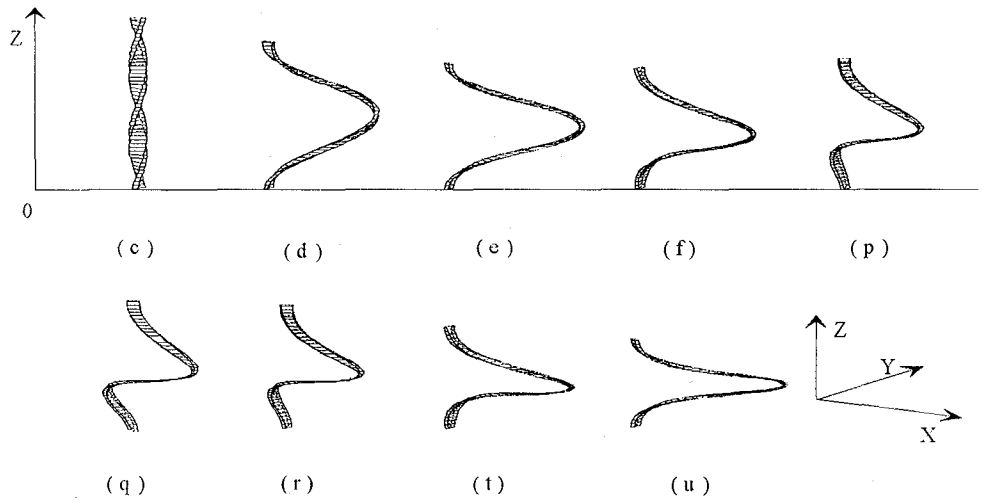

(a) Deformed modes on the first bifurcation path

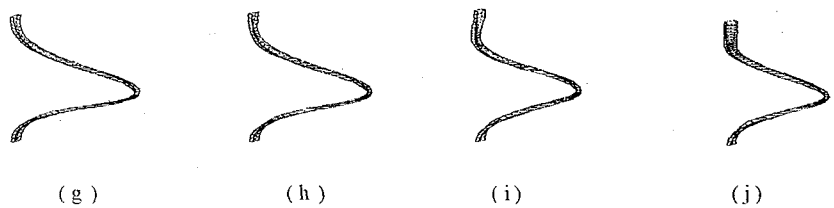

(b) Deformed modes on the secondary bifurcation path

Fig.10 Deformed modes

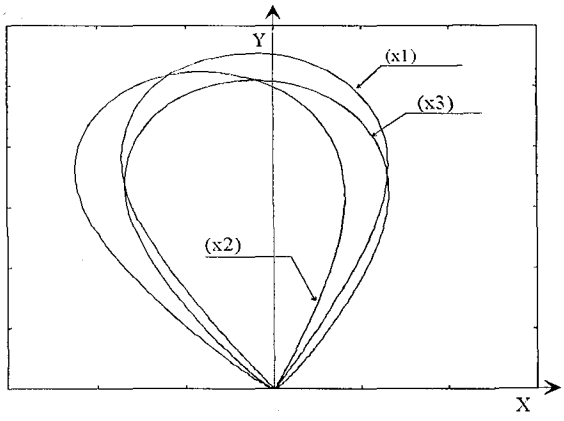

(a) Projections onto the X-Y plane

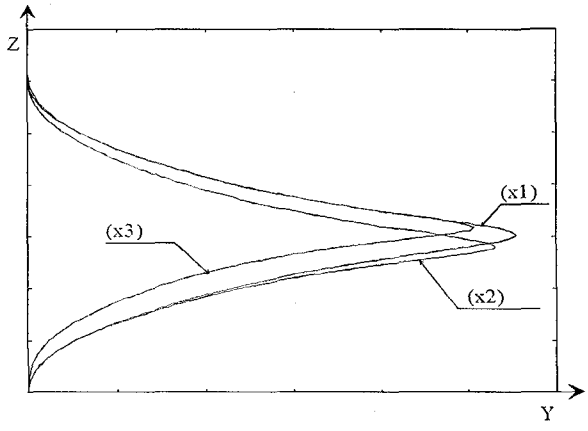

(b) Projections onto the Y-Z plane

Fig.11 Comparison of deformed modes of points (x1), (x2), (x3)

APPENDIX

(a).

$$[DR_1]=\begin{bmatrix} 1/2 & (\psi_2-\psi_1)\cos\bar{\theta}/4 & -\sin\bar{\theta}/2 \\ -(\psi_2-\psi_1)\cos\bar{\theta}\cos\bar{\phi}/4+(\theta_2-\theta_1)\sin\bar{\phi}/4 & (\psi_2-\psi_1)\sin\bar{\theta}\sin\bar{\phi}/4+\cos\bar{\phi}/2 & \cos\bar{\theta}\sin\bar{\phi}/2 \\ (\psi_2-\psi_1)\cos\bar{\theta}\sin\bar{\phi}/4+(\theta_2-\theta_1)\cos\bar{\phi}/4 & (\psi_2-\psi_1)\sin\bar{\theta}\cos\bar{\phi}/4-\sin\bar{\phi}/2 & \cos\bar{\theta}\cos\bar{\phi}/2 \end{bmatrix}$$

$$[DR_2]=\begin{bmatrix} -1/2 & (\psi_2-\psi_1)\cos\bar{\theta}/4 & \sin\bar{\theta}/2 \\ -(\psi_2-\psi_1)\cos\bar{\theta}\cos\bar{\phi}/4+(\theta_2-\theta_1)\sin\bar{\phi}/4 & (\psi_2-\psi_1)\sin\bar{\theta}\sin\bar{\phi}/4-\cos\bar{\phi}/2 & -\cos\bar{\theta}\sin\bar{\phi}/2 \\ (\psi_2-\psi_1)\cos\bar{\theta}\sin\bar{\phi}/4+(\theta_2-\theta_1)\cos\bar{\phi}/4 & (\psi_2-\psi_1)\sin\bar{\theta}\cos\bar{\phi}/4+\sin\bar{\phi}/2 & -\cos\bar{\theta}\cos\bar{\phi}/2 \end{bmatrix}$$

(b).

$$[Et_1]=\frac{1}{2}[E][D]\left[BR(\bar{\theta},\bar{\phi})\right]\left[BR(\theta_1,\phi_1)\right]^{-1}[R_1]$$

$$[Et_2]=\frac{1}{2}[E][D]\left[BR(\bar{\theta},\bar{\phi})\right]\left[BR(\theta_2,\phi_2)\right]^{-1}[R_2]$$

where

$$[E]=\begin{bmatrix} 0 & 0 & 0 & -c_1 & -c_2 & -c_3 & b_1 & b_2 & b_3 \\ c_1 & c_2 & c_3 & 0 & 0 & 0 & -a_1 & -a_2 & -a_3 \\ -b_1 & -b_2 & -b_3 & a_1 & a_2 & a_3 & 0 & 0 & 0 \end{bmatrix}$$

$$a_1=\cos\bar{\theta}\cos\bar{\psi},\quad a_2=\cos\bar{\theta}\sin\bar{\psi},\quad a_3=-\sin\bar{\theta}$$
$$b_1=-\cos\bar{\phi}\sin\bar{\psi}+\sin\bar{\phi}\sin\bar{\theta}\cos\bar{\psi},$$
$$b_2=\cos\bar{\phi}\cos\bar{\psi}+\sin\bar{\phi}\sin\bar{\theta}\sin\bar{\psi},\quad b_3=\sin\bar{\phi}\cos\bar{\theta}$$
$$c_1=\sin\bar{\phi}\sin\bar{\psi}+\cos\bar{\phi}\sin\bar{\theta}\cos\bar{\psi},$$
$$c_2=-\sin\bar{\phi}\cos\bar{\psi}+\cos\bar{\phi}\sin\bar{\theta}\sin\bar{\psi},\quad c_3=\cos\bar{\phi}\cos\bar{\theta}$$

and

$$[D]=\begin{bmatrix} u_2-u_1 & 0 & 0 \\ v_2-v_1 & 0 & 0 \\ w_2-w_1+l & 0 & 0 \\ 0 & u_2-u_1 & 0 \\ 0 & v_2-v_1 & 0 \\ 0 & w_2-w_1+l & 0 \\ 0 & 0 & u_2-u_1 \\ 0 & 0 & v_2-v_1 \\ 0 & 0 & w_2-w_1+l \end{bmatrix}$$

(c).

$$[R]=\begin{bmatrix} -[R_G] & [Et_1] & [R_G] & [Et_2] \\ [0] & -[DR_1]\left[BR(\theta_1,\phi_1)\right]^{-1}[R_1] & [0] & -[DR_2]\left[BR(\theta_2,\phi_2)\right]^{-1}[R_2] \end{bmatrix}$$

REFERENCES

1)Greenhill,A.G. (1883). *Proc. Inst. Mech. Engrs.*

2)Grammel,R. (1923). Das Kritische Drillungsmoment von wellen., *Math. Mech.*, Vol.3, pp.262

3)Ziegler,H. (1968). *Principles of Structural Stability*, Blaisdell Publishing Company.

4)Kurakata,Y. and Nishino,F (1982). Finite Displacement Field and Governing Equations of Solid Curved Beam, *Proc. of JSCE*, No.317, pp.15-30, Jan., 1982 (in Japanese)

5)Miura,K (1987). Space Structures and Applied Mechanics, *37th Japan NCTAM, Preprint.*

6)Natori,M. and Miura,K (1985). Deployable structures for space applications. *Proc.26th Structures,Structural Dynamics and Material Conference*, 1-9.

7)Natori,M. (1988). Experiment and Analysis of Three Dimensional Elastica.(in Japanese), *38th Japan NCTAM, 1988, Preprint.*

8)Love,A.E.H. (1944). *A Treatise on the Mathematical Theory of Elasticity*. Dover, New York.

9)Antman,S.S. (1972). The Theory of Rods. *Handbuch der Physik*, Vol.VIa/2. Springer, Berlin.

')Bathe,K.J. and Bolourchi,S. (1979). Large Displacement Analysis of Space Frames. *Int. J. Num. Methods Engng* 14, pp.961-986.

11)Maeda,Y. and Hayashi,M. (1976). Finite Displacement Analysis of Space Framed Structures. Proc. of JSCE. No.253, pp.13-27, Sept.,1976 (in Japanese).

12)Maeda,Y. and Hayashi,M. (1986). Finite displacement theory of solid curved beams, *J. of Struc. Engng*, Vol.32A, pp.139-151, (in Japanese).

13)Yoshida,Y., Masuda,N., Morimoto,T and Hirosawa,N. (1980). An Incremental Formulation for Computer Analysis of Space Framed Structures, *Proc. of JSCE*, No.300, pp.21-31, Aug., 1980 (in Japanese).

14)Ai,M. and Nishino,F (1982) A Theoretical Formulation of Thin-Walled Beam Elements within Small Strains under Finite Displacement, *Proc. of JSCE*, No.318, pp.7-20, Feb., 1982 (in Japanese)

15)Goto,S. (1983). A Formulation of Tangent Geometric Stiffness Matrix for Space Structure, *Proc. of JSCE*, No.335, pp.1-11, Jul., 1983 (in Japanese)

16)Goto,Y, Matsuura,S. and Hasegawa,A. (1985a) A Formulation of Finite Displacement Theory of Rod, *J. of Struc. Engng*, Vol.31A, pp.183-196,(in Japanese)

17)Goto,Y., Matsuura,S., Hasegawa,A. and Nishino,F. (1985b). A new formulation of finite displacement theory of curved and twisted rod. *Proc. of JSCE, Structural Eng./Earthquake Eng.*, Vol.2, No.2,pp.365s-375s, Oct. 1985.

18)Goto,Y., Morikawa,Y. and Matsuura,S. (1988). Direct Lagrangian nonlinear analysis of elastic apace rods using transfer matrix technique. *Proc. of JSCE, Structural Eng./Earthquake Eng.*, Vol.5. No.1, pp151s-160s, Apr. 1988.

19)Goto,Y., Suzuki,S. and Chen,W.F. (1991). Analysis of critical behavior of semi-rigid frames with or without load history in connections. *Int. J. Solids Structures*. Vol.27, No.4, pp.467-483,1991.

20)Simo,J.C.and Vu-Quoc,L.(1986). A three- dimensional finite strain rod model--Part II : Computational aspects. *Comput. Meths. Appl. Mech. Engng* **58,** pp.79-116.

21)Iura,M. and Hiroshima,M. (1986). Geometrically Nonlinear Theory of Naturally Curved and Twisted Rods Undergoing Finite Rotations, *J. of Struc. Engng*, Vol.32A, pp.153-163, (in Japanese).

22)Iura,M. and Aturi,S.N. (1989). Dynamic Analysis of Naturally curved and Twisted Rods with Finite Rotations, *J. of Struc. Engng*, Vol.35A, pp.165-174, (in Japanese).

23)Iwasaki,E and Hayashi,M. (1991). On the refinement of finite displacement analysis of space framed structures, *J. of Struc. Engng*, Vol.37A,pp.353-366,(in Japanese)

24)Goto,Y., Watanabe,Y., Kasugai,T., and Obata,M. (1992). Elastic Buckling Phenomenon Applicable to Deployable Rings. *Int. J. Solids Structure*, Vol.29, No.7, pp.893-909.

25)Ai,M. and Nishino,F (1980). Mechanics in geometrically nonlinear problem of discrete system and application to plane frame problem, *Proc. of JSCE*, No.304, pp.17-32, (in Japanese).

26)Kasugai,T.(1993). Refined numerical methods and their accuracy for the finite displacement analysis of frames. (in Japanese), Dr. of Eng. Thesis. Dept. of Civil Eng. , Nagoya Institute of Technology.

27)Timoshenkio,S.P. and Goodier,J.N. (1970). *Theory of Elasticity*, pp.291-353, McGraw-Hill, Maidenhead.

(Received September 14, 1994)